Earth Planets Space, **53**, 75–89, 2001

Three-component OBS-data processing for lithology and fluid prediction in the mid-Norway margin, NE Atlantic

Eivind Berg[1*], Lasse Amundsen[1], Andrew Morton[1*], Rolf Mjelde[2], Hideki Shimamura[3], Hajime Shiobara[3**], Toshihiko Kanazawa[4**], Shuichi Kodaira[3***], and Jan Petter Fjellanger[2****]

[1]*Statoil, Trondheim, Norway*
[2]*Inst. of Solid Earth physics, University of Bergen, Norway*
[3]*Inst. for Seismology and Volcanology, Hokkaido University, Sapporo, Japan*
[4]*Lab. Earthquake Chemistry, Tokyo University, Japan*

(Received January 24, 2000; Revised September 25, 2000; Accepted October 18, 2000)

In 1992, a comprehensive three-component ocean bottom seismic survey was performed in the central and northern area of the Vøring Basin, offshore mid-Norway, NE Atlantic. An important part of the data acquisition program consisted of a local survey with 20 Ocean Bottom Seismographs (OBS) dropped at approximately 200 m interval in 1300 m water depth. The main purpose of the local survey was to acquire densely sampled P- and S-wave reflection data above a seismic flatspot anomaly observed earlier, in order to more accurately predict if hydrocarbons could be related to it. The conventional reflection data processing methods applied to the vertical components included predictive deconvolution in order to attenuate low frequency ringing, near offset mute and a series of constant velocity stacks in order to obtain the optimal velocity function. The final result is a "trouser" shaped, high resolution V_z stacked section with minor influence of water multiples. The inline (V_x) component contains no strong multiples, and extensive near trace muting was hence not necessary to apply for this component. Velocity analysis together with ray-tracing modelling indicate that P-S-converted shear waves (reflections) represent the dominant mode. The results of the interpretation and modelling indicated a V_p/V_s-ratio of approximately 2.6 in the overburden, which suggests domination of partly unconsolidated shale, while the V_p/V_s-ratio in the assumed reservoir was approximately 1.8, which indicates a more sand dominated facies. Outside the flatspot area a higher V_p/V_s-ratio ratio (approximately 2.0) was estimated, indicating that hydrocarbons could be present in the assumed reservoir.

1. Introduction

Recording the seismic wavefield at the sea-floor using multicomponent receivers has several advantages compared to conventional near surface recording (Caldwell, 1999); improved P-wave imaging due to lower background noise level, better azimuth distribution and more possibilities for removal of receiver ghost and multiples, use of P-S-converted waves to image below shallow gas and to map geological boundaries with low acoustic impedance for P-waves.

Furthermore, it is well known that obtaining estimates of S-wave velocities for sedimentary rocks in addition to P-wave velocities to a certain extent enables prediction of lithology and fluids (e.g. Nur and Simmons, 1969; Christensen and Fountain, 1975; Spencer and Nur, 1976; Kern, 1982; Christensen, 1984; Crampin, 1990). In several different sedimentary sequences it has been shown that the V_p/V_s-ratio can be related to the sand/shale ratio; a V_p/V_s-ratio of 1.6 representing sand and a V_p/V_s-ratio of 2.0 representing shale. Presence of hydrocarbons tend to decrease the V_p/V_s-ratio (Neidell, 1985).

The V_p/V_s-ratio can be estimated indirectly from marine seismic data by analysing Amplitude-Versus-Offset (AVO), but in order to perform more precise direct measurements, three-component (3-C) recorders on the ocean bottom are needed. In 1992 a comprehensive 3-C OBS (Ocean Bottom Seismograph) survey was performed in the central and northern area of the Vøring Basin, mid-Norway margin, NE Atlantic, the largest sedimentary basin off Norway remaining to be explored (Fig. 1). The data acquisition program consisted of three parts, with one regional and one semi-regional part providing the large basin coverage (Digranes *et al*., 1996; Mjelde *et al*., 1996, 1997a, b). The third part consisted of a local survey with 20 OBSs dropped along surface seismic line VB-08-89 at approximately 200 m interval in 1300 m water depth (Fig. 2). The main purpose of the local survey was to acquire densely sampled P- and S-wave reflections above a seismic flatspot anomaly observed earlier in surface seismic data, in order to more accurately predict if hydrocarbons could be present. Flatspots are often taken as indicators of the presence of hydrocarbons, and they are interpreted as boundaries between different types of pore-fluid, e.g. gas and water (Caldwell, 1999). The survey was undertaken by sci-

*Now at SB Geophysical a.s., Trondheim, Norway.
**Now at Earthquake Research Inst., Tokyo University, Japan.
***Now at JAMSTEC, Yokosuka, Japan.
****Now at Norsk Hydro, Bergen, Norway.

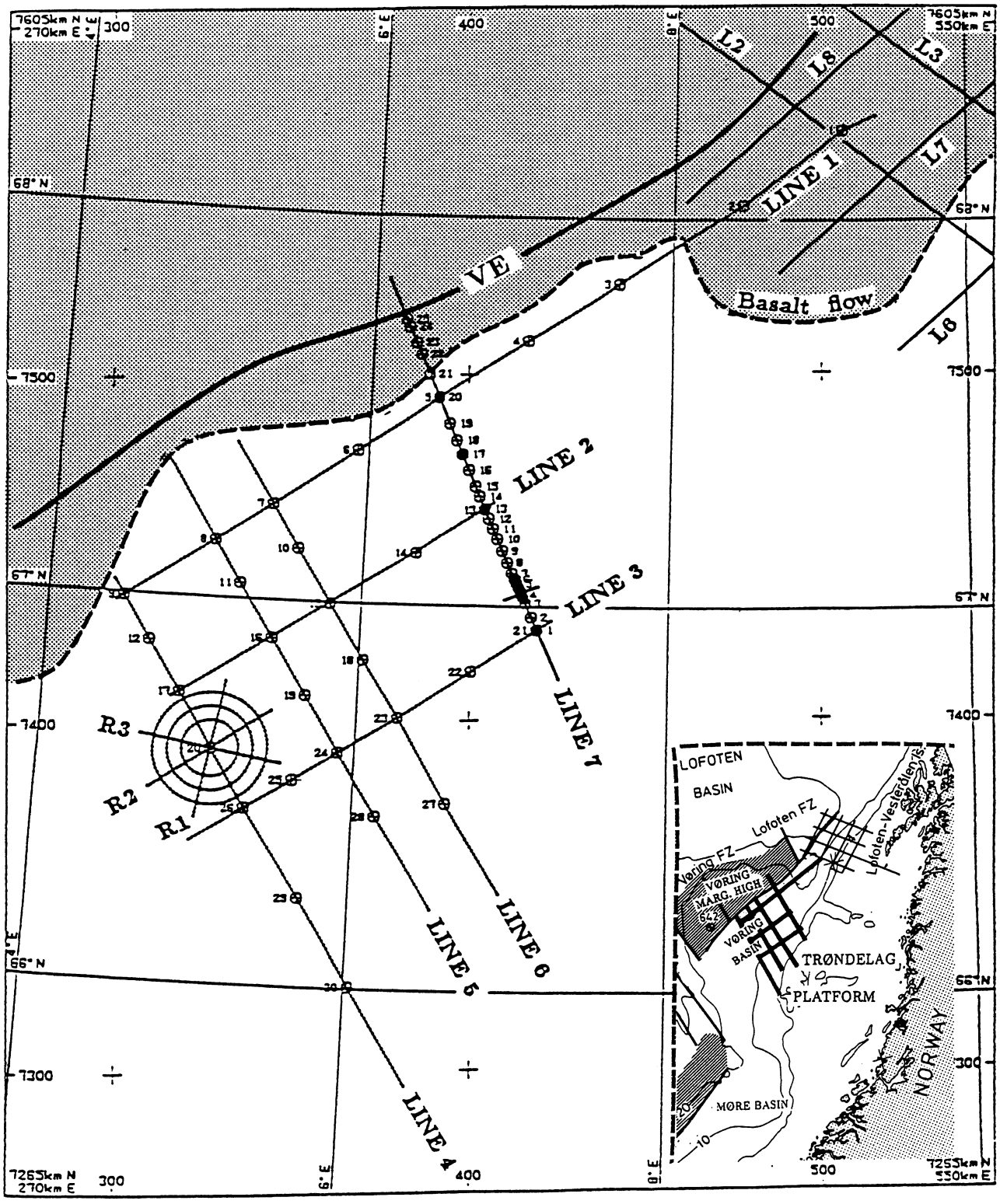

Fig. 1. Location of the OBS-profiles acquired during the survey in 1992. The local data presented in this paper were acquired along a part of Line 7. The framed area shows the geographical location of the 1992 profiles (bold lines), as well as regional OBS-profiles acquired off Lofoten in 1988 (thin lines). VE = Vøring Escarpment.

entists from the Universities of Bergen, Hokkaido and Tokyo as well as from Statoil's Research Centre in Trondheim. The data were converted from its original analogue tape format to a standard digital format at Hokkaido University. Further processing (described in this paper) has been applied using Advance Geophysical's (now Landmark's) ProMAX and VSP software in Statoil's Research Centre to produce stacked seismic sections of the vertical and inline horizontal components of the data.

The main objective of the present paper is to demonstrate

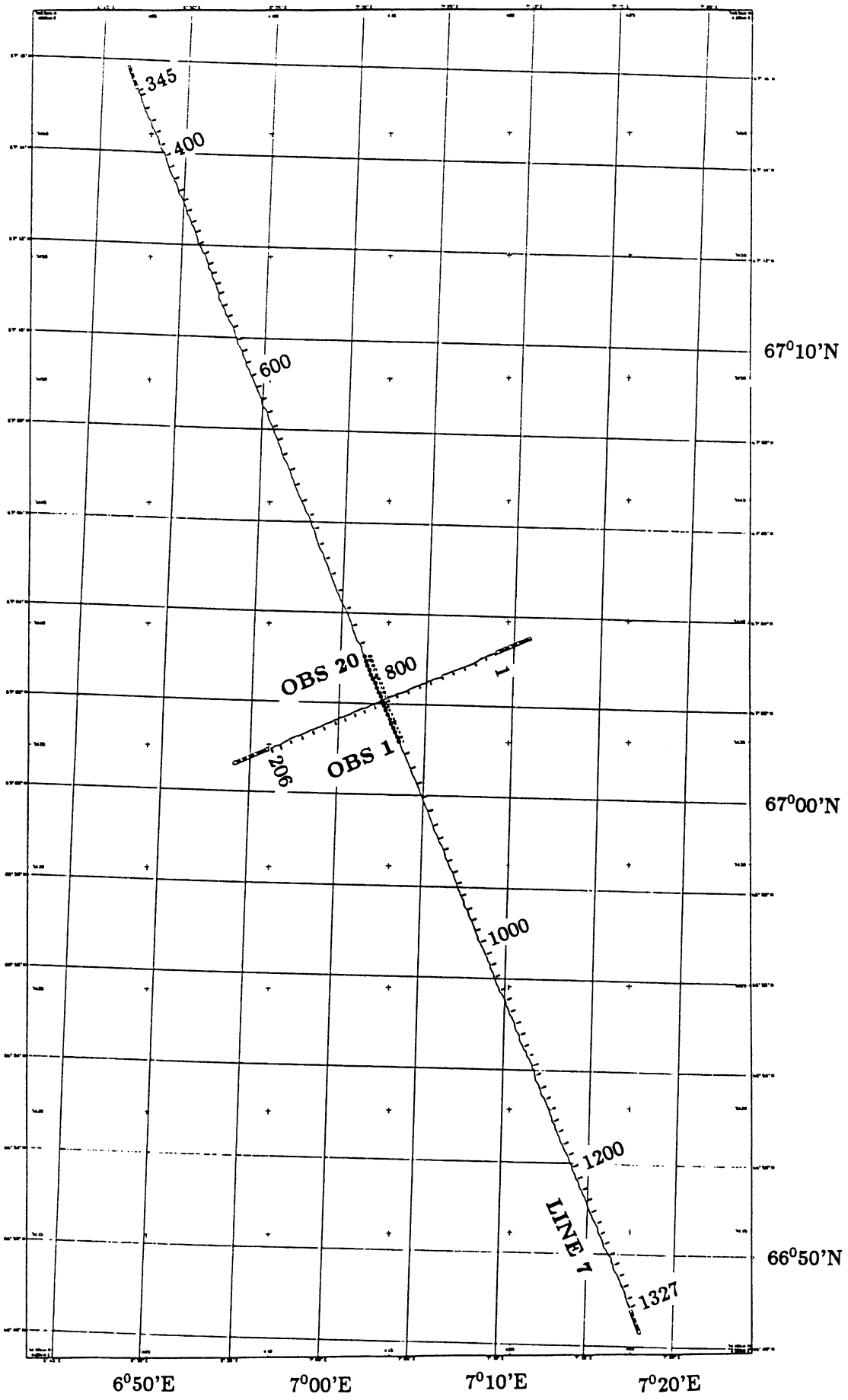

Fig. 2. Shotpoint map of the local survey. The data from the short perpendicular profile (shotpoint 1–206) have not been included in the present study.

Table 1. Surface coordinates (UTM) and shotpoint numbers of OBS locations on reflection profile VB-08-89.

OBS	SP	*X*	*Y*
1	3627	415409	7435101
2	3619	415332	7435288
3	3611	415252	7435474
4	3604	415182	7435645
7	3579	414954	7436213
8	3571	414873	7436399
9	3563	414794	7436581
10	3555	414722	7436764
12	3539	414570	7437136
13	3531	414492	7437322
14	3524	414425	7437485
15	3515	414341	7437690
16	3507	414262	7437888
17	3499	414193	7438061
18	3491	414120	7438247
19	3483	414045	7438437
20	3476	413970	7438612

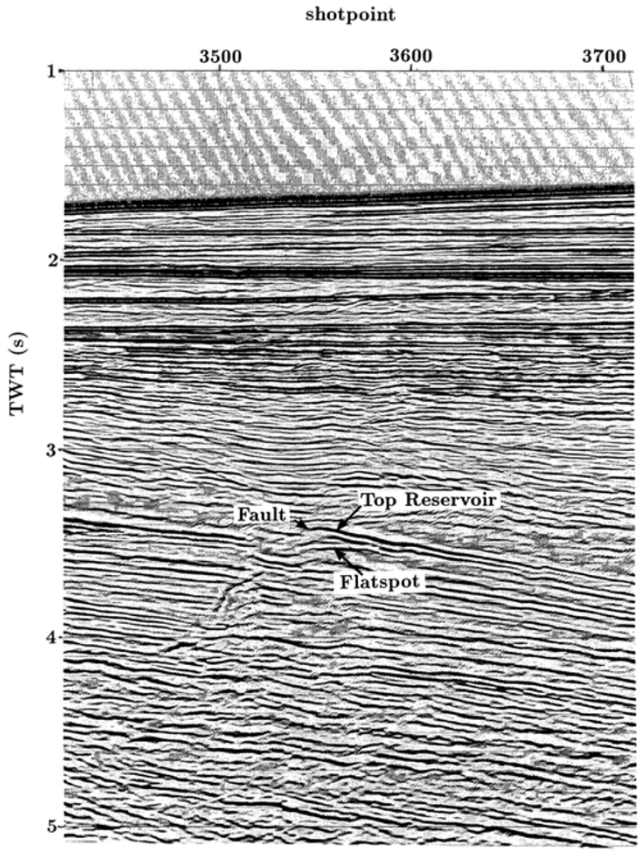

Fig. 3. Part of reflection profile VB-08-89 (migrated stack processed by Merlin Geophysical). The OBSs in the local study were located above the indicated flatspot. The reservoir is assumed to be bounded by the flatspot, the intra Campanian Unconformity (top reservoir) and the fault.

how conventional (surface) reflection data processing methods applied to 3-C OBS-data can be used for lithology and fluid predictions.

2. Data Acquisition

The OBSs used in the survey were developed at Laboratory for Ocean Bottom Seismology, Hokkaido University, and Laboratory for Earthquake Chemistry, Tokyo University (Shimamura, 1988; Kanazawa, 1993). Each OBS contains gimbal-mounted, oil damped, three-component geophones, two variable speed tape drives, an amplifier with gain settings of 49 dB and 79 dB, and an internal clock calibrated to a master clock onboard the vessel. Other equipment, such as ballast, a release mechanism and homing aids, are incorporated for the deployment and retrieval of the instruments.

For the data presented in this paper, the analogue seismic signals were recorded with a high tape drive speed, allowing frequencies up to 40 Hz to be preserved, and the OBSs to remain active on the sea-floor for almost 8 days. As the OBSs were deployed in deep water (ca. 1300 m depth), the ballast was increased to 40 kg to speed up their descent and prevent the instruments from drifting laterally too far from the release point on the surface. Their position on the sea bed was obtained by measuring the ship to transponder distance from 19 different surface positions, using a measured acoustic velocity-depth function and then performing non-linear inversion to minimise the travel time errors between observed and ray-traced times (Shiobara *et al.*, 1997). The

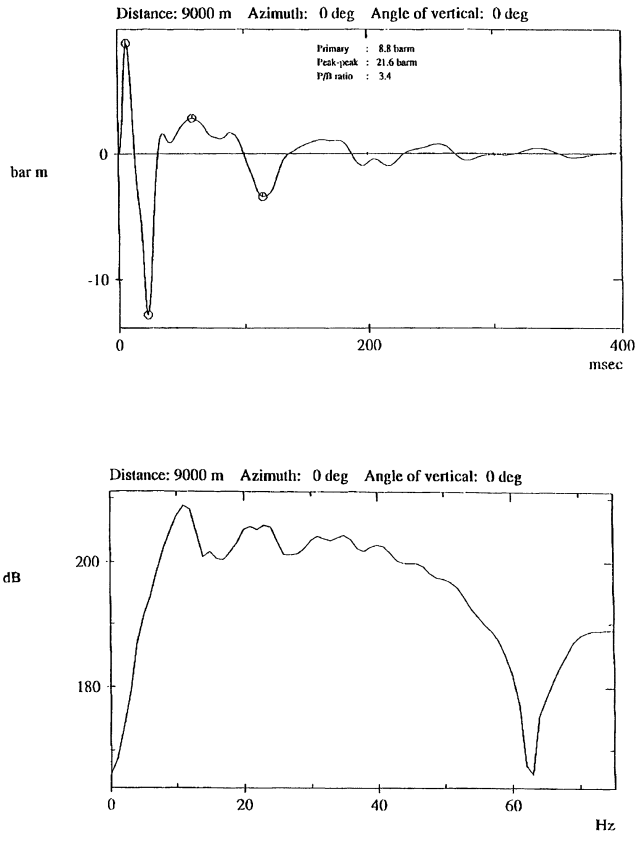

Fig. 4. Theoretical seismic pulse (far-field signature; above) and theoretical amplitude spectrum (below) of the air-gun array employed.

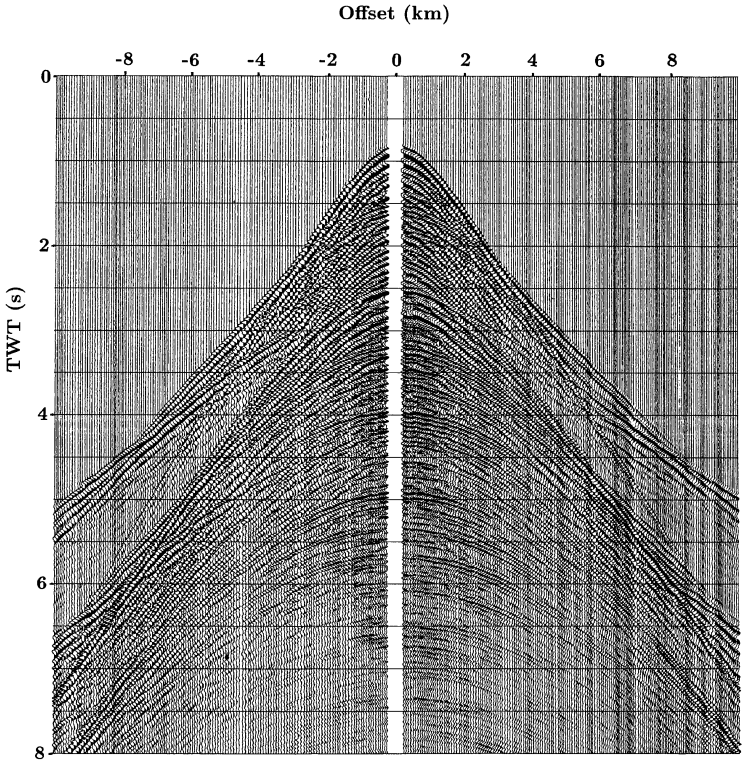

Fig. 5. Raw data recorded on the vertical component of OBS 10.

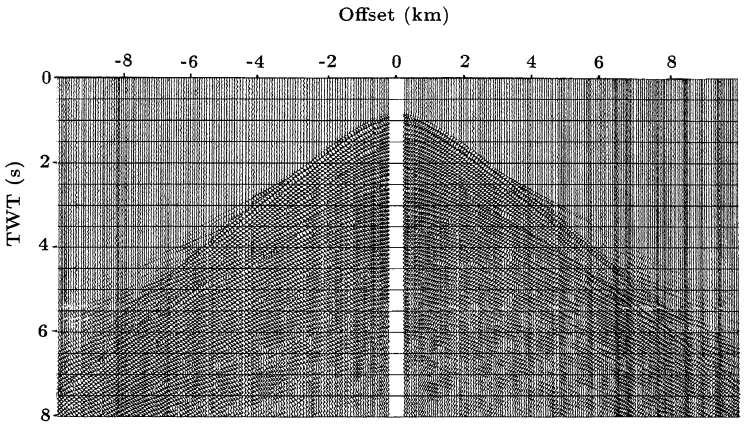

Fig. 6. Raw data recorded on one of the horizontal components of OBS 10. (The data on the other horizontal component is qualitatively very similar and is hence not presented).

true OBS positions were generally found to be at distances less than 100 m from their deployment positions with an error in the positioning of about 10 m. 20 OBSs were deployed along the position of line VB-08-89 with an approximate separation of 200 m (Fig. 2; Table 1), centered above the flatspot indicated in Fig. 3.

The data presented in this paper were recorded in the high gain setting using an air-gun array (7 air-guns) with a total volume of 32.1 l (1956 in^3) towed at a depth of 12 m. The source signature and amplitude spectrum are shown in Fig. 4. During the shooting of the ca. 56 km long line the vessel attempted to maintain a constant speed of 1.6 knots and fire the guns every 60 seconds, corresponding to ca. every 50 m. However, this speed was not maintainable in strong currents, and the speed of the vessel had to be gradually increased to 2.8 knots.

3. Multicomponent OBS Processing

3.1 Data input

The analogue data was first decomposed into sequential shot ordered data and digitised by reference to a time-signal recorded on an auxiliary channel along with the three data channels, one for each component. The sample rate of the data was 5 ms. Only 17 datasets were recovered from the 20 OBSs deployed. The data for positions 5 and 6 were lost since the OBSs could not be released from the sea bed and re-

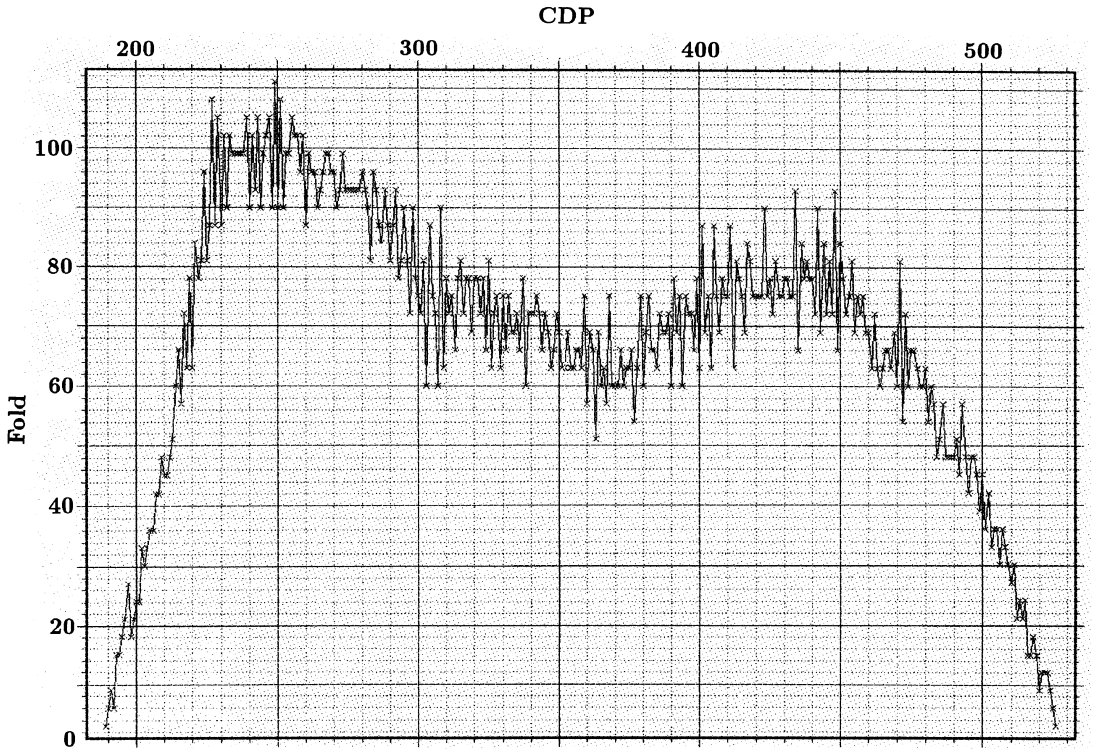

Fig. 7. Fold of stack for CDP line.

covered, and the data for OBS 11 was discarded as it appeared very noisy due to problems with the gain settings. The raw data for the vertical and one of the horizontal components of OBS 10 are presented in Figs. 5 and 6.

Initially each tape was read into ProMAX, preserving the offset and field file numbers in the trace headers. From each of the field files channels 1–3 were extracted: channel 2 being the vertical component and channels 1 and 3 the two perpendicular horizontal components. After studying some of the common OBS gathers, the input data were further limited to a maximum offset of 15 km and a time of 12 s. For each OBS a dataset was created with a surface shot point and coordinate relative to the conventional seismic line acquired in 1989 (VB-08/08A-89). This provided the basis for a line geometry, which was needed to obtain a stack from the data. Table 1 shows the shot point numbers and coordinates used. By creating a geometry and combining the 17 OBS datasets into one, it was possible to extract individual components and attempt to process the data with conventional techniques.

3.2 Geometry application

The next step in the processing sequence consisted of creating the geometry necessary for processing and stacking the data. The detailed procedure for the geometry application is presented in Appendix A.

For this dataset the average fold for 50 m bin width is around 80, if all offsets are included in the stack (Fig. 7). Discarding traces not contributing to the stack at the target level leaves a fold of stack of around 25.

For asymmetric or Common Conversion Point (CCP) binning of the horizontal components, the calculation of the CCP x coordinate includes constants derived from the V_p/V_s-ratio. The CCP formula used is:

$$\mathrm{CCP} = \frac{2}{V+1} Source + \frac{2V}{V+1} Receiver \qquad (1)$$

where

$$V = \frac{V_P}{V_S}. \qquad (2)$$

When the V_p/V_s-ratio equals one, this equation gives normal CMP numbering. A geometry was created for the horizontal component data with a V_p/V_s-ratio of 1.0, 1.75, 2.0, 2.5 and 2.75.

3.3 Processing of the vertical component

The first attempts to identify the flatspot were in the receiver domain of the vertical components. Some efforts were made to NMO correct these gathers both with a velocity function taken from the VB-08/08A-89 migrated stack, and a simplified velocity function based on four key horizons identified in the gathers. An attempt to stack the data (in the receiver domain) before the geometry was created, indicated that the flatspot could be identified if the multiple energy was removed. As the spatial sampling is irregular, multiple attenuation can only be accomplished by inner trace muting. This first simple stack (Fig. 8) showed the major horizons and a dipping event interpreted as the intra Campanian unconformity (Mjelde *et al.*, 1997a) located above the flatspot, which cannot be seen clearly.

Once the geometry had been applied and trace mid points were assigned to a location, the data could be stacked in a more conventional sense. Further pre-stack processing was applied in order to try to enhance the continuity of arrivals, but because of the spatial sampling limitations it could only be performed trace by trace. The optimum deconvolution

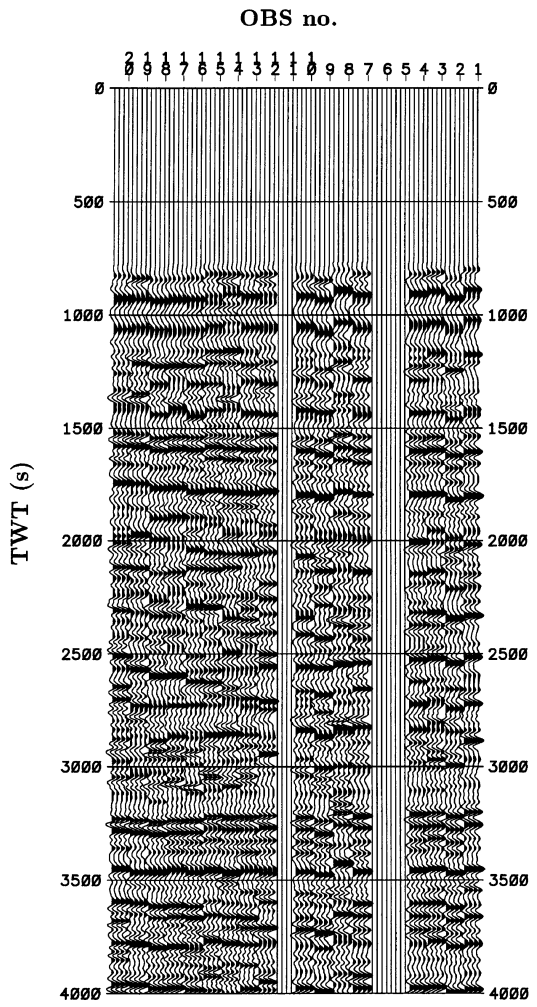

Fig. 8. Initial "receiver gather" stack (after application of deconvolution; see Fig. 10). The stacked trace for each OBS has been displayed four times.

parameters found were a 250 ms operator with 50 ms gap for predictive deconvolution. After analysing the OBS amplitude spectra (Fig. 9), a minimum phase Butterworth band pass filter of 5 to 35 Hz with slopes of 18 and 72 dB/octave was applied. Figure 10 shows the vertical component of OBS 10 after application of deconvolution and band pass filtering.

Top and bottom mutes were individually picked on the OBS gathers to remove the high-energy direct arrivals and the sea bottom multiple (Fig. 11). The resulting "trouser" shaped stack has strongly improved primary signal around the target interval at 2700 ms. Figure 12(a) shows a stack of the data with a single velocity function taken from VB-08/08A-89. With these parameters applied to a CMP-sorted dataset, it was possible to perform velocity analysis and a much more detailed velocity field could be picked. The locations for the analysis were, on average, every 10th CMP (500 m) and the analysis was performed on a super gather of 5 CMPs, summed with a 50 m offset bin. This improved the offset sampling to give a more regularly sampled gather and hence a better velocity analysis. The velocity function was picked on a normalized semblance display, with an interactive stack and gather for quality control. The gather display was difficult to utilize due to the muting and sampling, and the velocity functions were generally difficult to pick consistently due to the low fold of the primary energy. The difference in semblance between signal and noise was slight, and the display (colour contouring) and scaling (time normalising) was thus important. Figure 13(a) shows a typical semblance display taken from the data. Constant velocity stacks were run on the whole line to help distinguish events, and a simple velocity field was derived from them. As the quality of the picking was difficult to evaluate during the analysis, and the data are very sensitive to muting (especially the top mute) and velocity, it was found that the best test of a velocity field and/or mute was to actually perform the stack.

In the CMP domain it is also possible to derive and apply trim statics before stacking. These simple correlation statics are derived along a horizon-following window. CMP trim statics provide a powerful tool to optimise the stack, but the result is heavily dependant on the parameters chosen. Different horizons were selected, but the event at 1500 ms with a 3000 ms window over 3 CMPs provided the most consistent results. The maximum static allowed was set to 40 ms, and during the analysis many traces reached this limit. It was found that a better stack was obtained if those traces that reached the maximum had their static shift set to zero. Figure 12(b) shows a residual corrected stack. Once a reasonable set of statics was derived, velocity analysis was performed on a residual corrected dataset, and the velocity field was finely tuned. Efforts to improve the post stack data were made, since these data represent regular zero offset traces at 50 m increments. F-X deconvolution (random noise removal) and post stack F-K filtering (dipping noise attenuation) were performed, but did not produce any significant improvement.

From the vertical component stack it can be seen that the event at roughly 1500 ms is approximately flat. Picking a horizon along this event allows a static shift to be applied using the "Horizon Flattening" tool (Fig. 12(c)). This improves the overall appearance of the events, the flatspot appears more horizontal, and the stack ties better with the conventional surface seismics. The stack with residual statics and the F-K filter was finally migrated with an Explicit Finite Difference Time Migration algorithm, as shown in Fig. 12(d).

3.4 Processing of the horizontal components

Considerable efforts were made in order to rotate the horizontal components into inline and crossline components. This work is described in detail in Appendix B. Since this study was not conclusive, both the unrotated and rotated datasets have been used in the further processing. The processing of the horizontal components has been performed both with regards to SS and PS waves. SS waves are the mode P-S-converted near the sea-floor on the way down, and PS waves represent the mode P-S-converted upon reflection.

Most of the initial processing work on the horizontal components was concentrated on the unrotated dataset, of which the one with the highest RMS level was assumed to represent the X component. This dataset was sorted into CMP order (a V_p/V_s-ratio 1.0) and velocity analysis was performed subsequently. The strong multiples present in the vertical component are absent in the horizontal components, and the severe inner trace mute was thus not needed for these components.

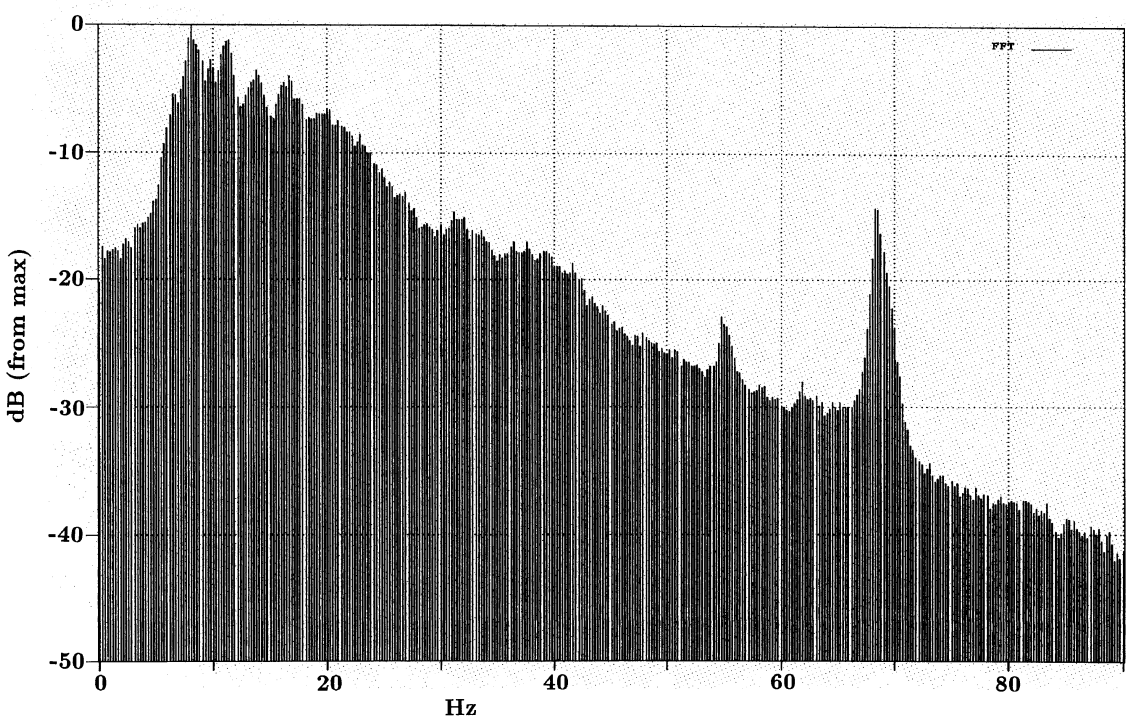

Fig. 9. Amplitude spectrum of the vertical component of OBS 10. The spikes at 55 and 68 Hz can most likely be attributed to instrumental noise.

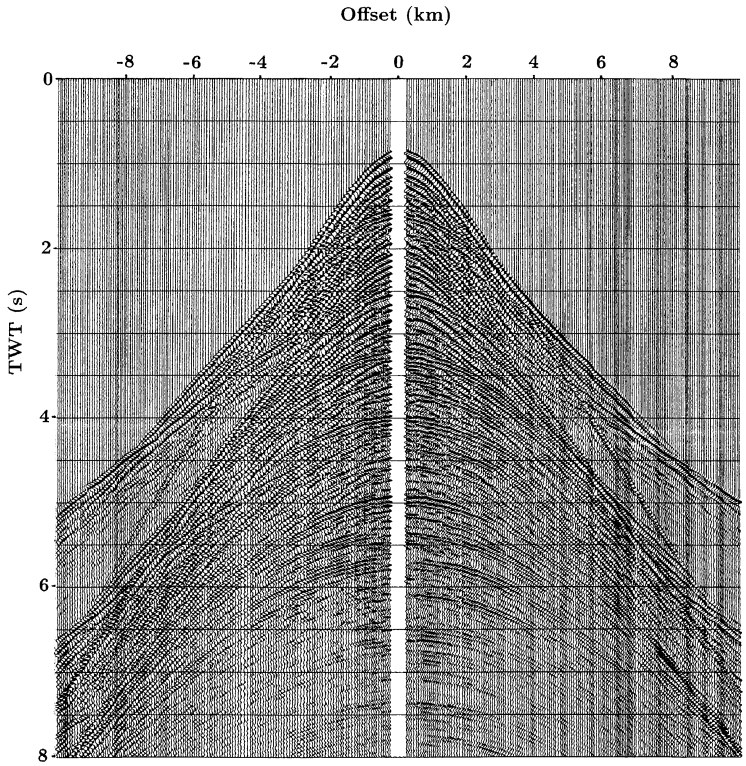

Fig. 10. The data for the vertical component of OBS 10 after minimum phase predictive deconvolution (250 ms operator length, 50 pred. dist.) and bandpass filtering (5-18-35-71 Hz).

As for the Z component, the data were found to be very sensitive to velocities and mute, and quite different stacks were produced from small variations in these parameters. The velocity analysis was also performed on datasets containing the separated positive and negative offsets, as stacking the data showed that this produced differences. Displaying whole line constant velocity stacks helped to guide the picking, as the data quality is not as good as for the Z com-

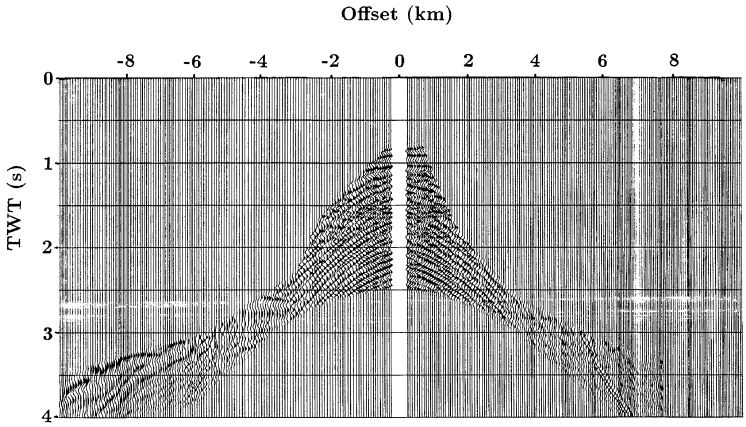

Fig. 11. Filtered data for the vertical component of OBS 10 after NMO correction and muting.

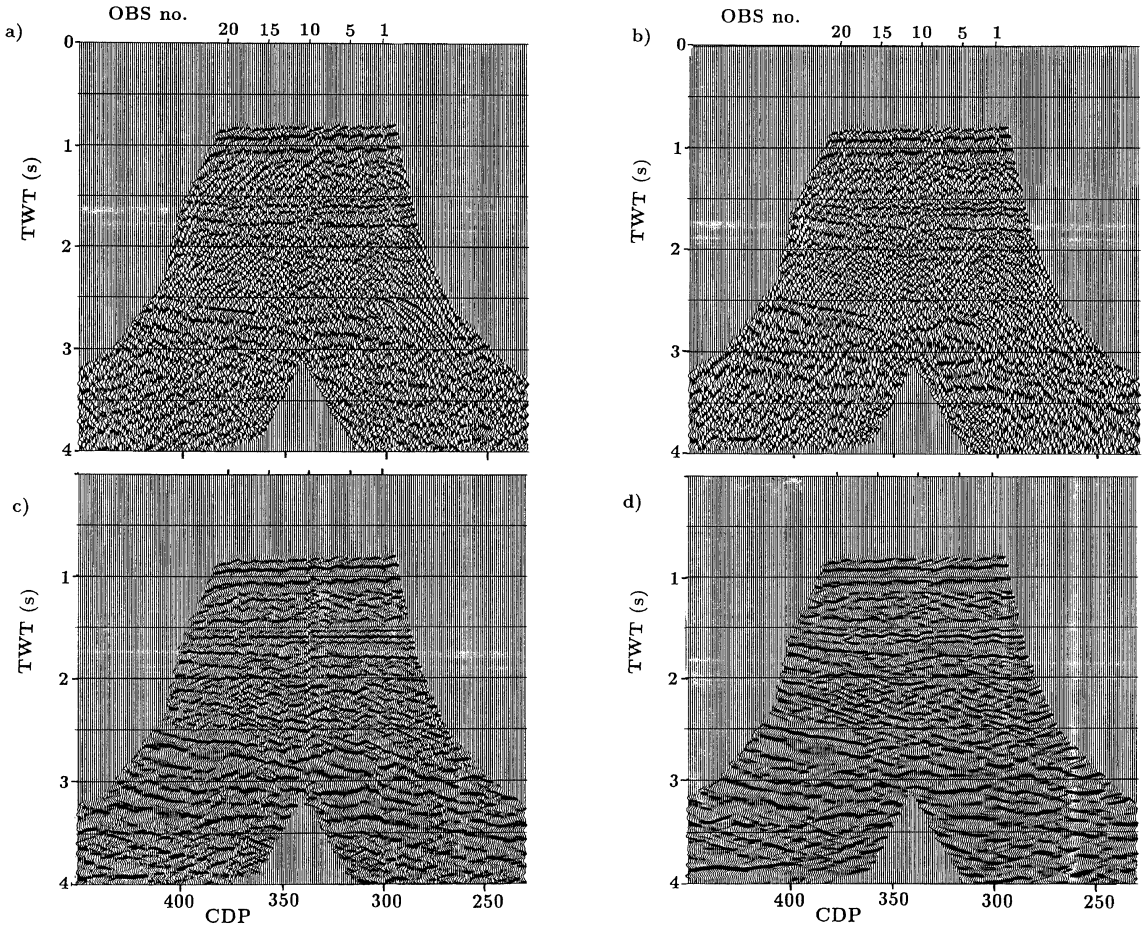

Fig. 12. Vertical component stack (pred. decon. 250/50 ms, 50 m CMP binning). a) Single velocity function from reflection profile VB-08/08A-89. b) With residual (CDP trim) statics. c) With horizon flattening and post stack FK. d) Migrated stack (Explicit Finite Difference Time Migration).

ponent, and the semblance plots are much more difficult to interpret (Fig. 13(b)). In addition to velocity analysis on conventional CMP sorted data, such analysis was also performed on datasets with asymmetric binning (CCP sorted); with V_p/V_s-ratios of 1.75, 2.5 and 2.75.

The data were stacked with the various velocity fields and mutes, but the sections do not appear as coherent as the vertical component stack, and as for land processing, the data appear affected by statics. These characteristics are also seen on the rotated dataset, so unless the quality of the rotation is poor, they are not caused by the relative orientations of the OBSs. Events which do not appear consistent across a stack or have high frequency structural variations should generally be improved by some kind of shot/receiver domain residual

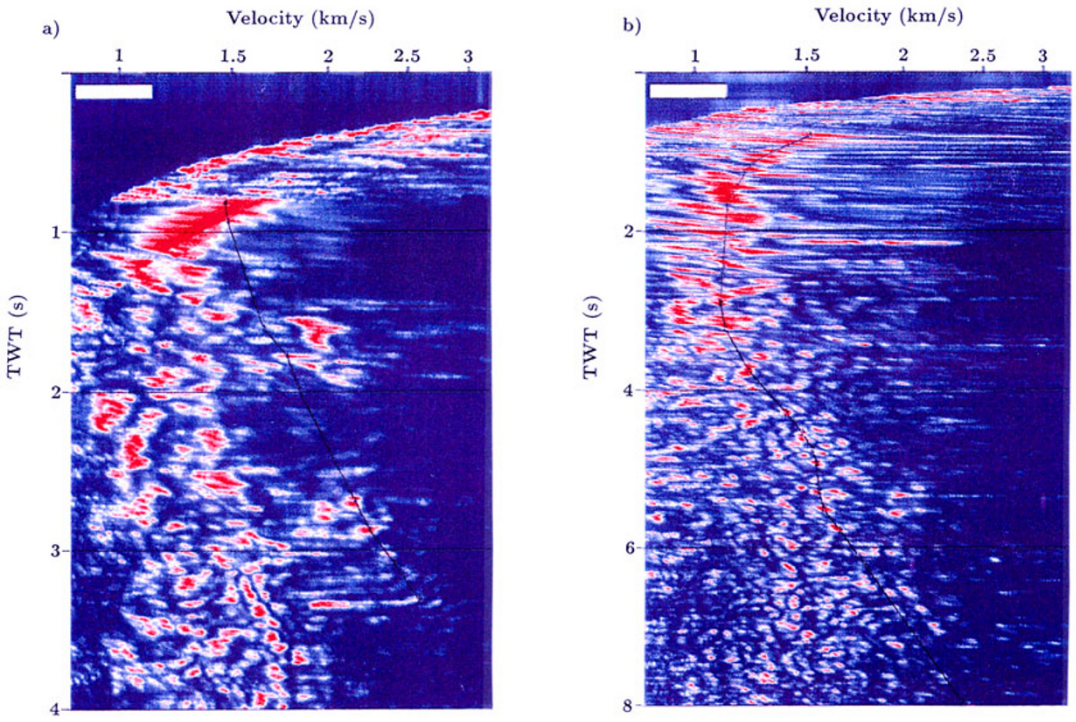

Fig. 13. a) Typical vertical component semblance plot. b) Typical horizontal component semblance plot.

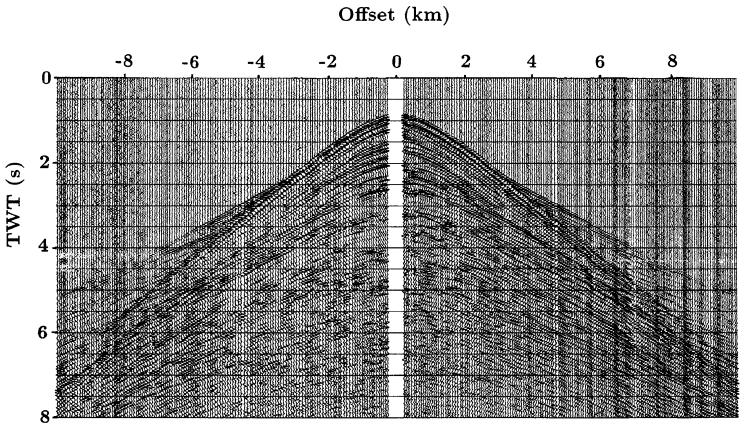

Fig. 14. Inline (X) horizontal component of OBS 10 after minimum phase predictive deconvolution (250 ms operator length, 50 pred. dist.) and bandpass filtering (5-18-35-71 Hz).

statics program. However, in this case there should be no shot statics as we have a marine source, and we have furthermore only minor knowledge about the near surface of the sea bed. The fold of coverage in the shot and receiver domain is poor, and any static would also contain some error due to the approximations made in the geometry and positioning. As no shot/receiver domain residual statics can be calculated, CMP or CCP trim statics were attempted. The absence of any strong, consistent event to guide the correlation window produced erratic statics, and any improvements in the stacks were negligible.

The post stack processes used on the vertical component were also applied to the horizontal stacks. F-X deconvolution removed random noise and increased the level of higher frequencies, but the F-K filter degraded the stack, producing a rather smeared out section. Without a consistent event it was not possible to use horizon flattening, and even the sea bed (or direct arrival) was not coherent enough to be utilized. The final stacks were displayed with the same filter and scaling as for the vertical component; Figs. 16(a) and (b) show an example of CMP and CCP stacks with FX deconvolution.

3.5 Interpretation and modelling

The final processed vertical (V_z) and inline (V_x) sections are displayed in Figs. 17 and 18, respectively. The horizontal CCP stack (Fig. 16(b)) has been chosen, since it provides the best correlation with events in the vertical stack. The interpretation of the sections depends strongly on accurate event correlation with the surface seismic data and identification

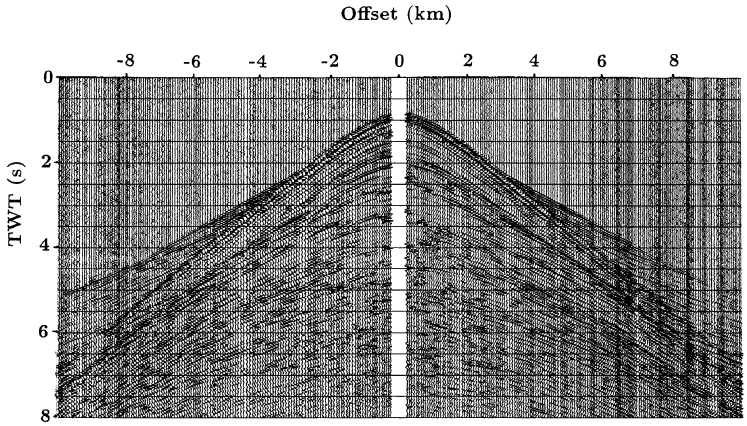

Fig. 15. Crossline (Y) horizontal component of OBS 10 after minimum phase predictive deconvolution (250 ms operator length, 50 pred. dist.) and bandpass filtering (5-18-35-71 Hz).

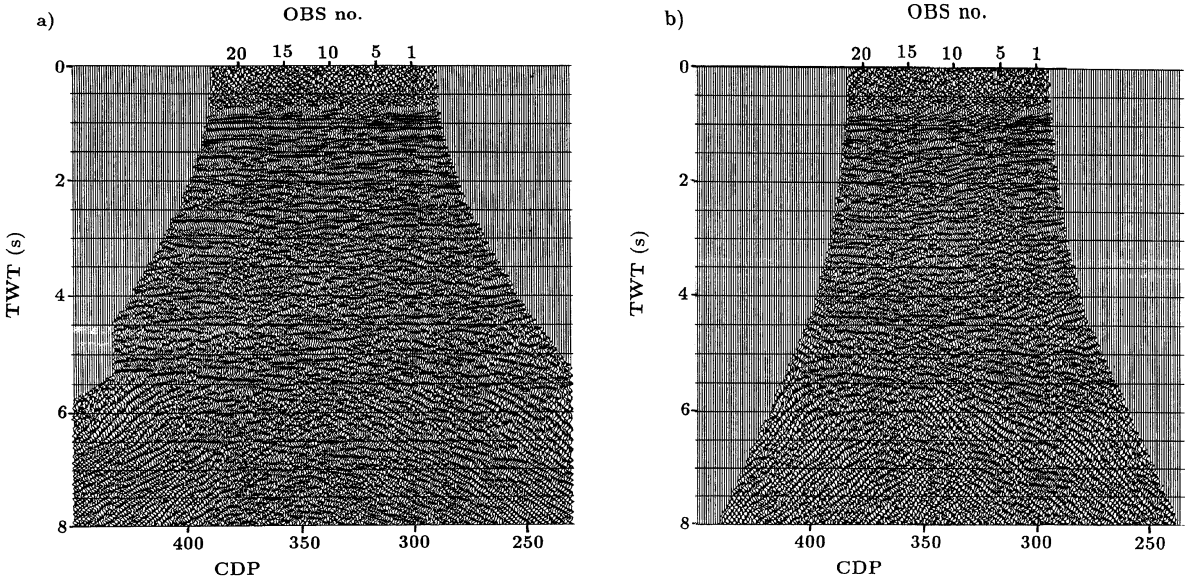

Fig. 16. Inline (X) horizontal component stack (pred. decon. 250/50 ms, 50 m CMP binning). a) CMP stack with FX deconvolution. b) CCP (V_p/V_s-ratio of 2.5) stack with FX deconvolution.

of events and seismic patterns on the inline component. No wells are available for calibration or data correlation. The stacked V_z-section can be considered as a P-wave section, and correlates as expected well with the surface seismic data (Fig. 3). The top reservoir (Intra Campanian) and the flatspot anomaly are easily identified in these data sections. Also the structural features with dipping layers and the graben immediately west of the anomaly can be observed.

The processing and modelling of the V_x component suggested that P-to-S converted reflections represent the dominant mode, and the detailed processing of this component focused consequently on enhancing P-to-S conversions. These results are consistent with recent synthetic modelling performed by Rodriguez-Suarez *et al.* (2000). The top reservoir reflector can be observed as the first strong dipping reflector at approximately 4500–5000 ms. The flatspot anomaly can also be observed in the converted data, even though it is not as clear as on the V_z-section. The fact that the flatspot can be (weakly) observed also for S-waves may suggest that the anomaly does not correspond to a pure fluid contact, as this should normally cause absence of mode conversions at the anomaly. The presence of the anomaly in the horizontal stack might indicate diagenetic changes across the fluid contact, although it should be emphasized that density variations alone in fluids could cause mode conversions.

To support the interpretation and identify the most important P- and S-wave arrivals, ray-tracing was performed. A 2-D model for the OBS line was built from interpreted surface seismic data and RMS-velocity picks on CMP gathers. P-wave interval velocities were estimated from the RMS velocities. A model showing the main layers is displayed in Fig. 19(a). Figure 19(b) shows a spikeogram, generated with the NORSAR-2D ray tracing package, for an OBS location at horizontal reference distance 13.8 km. The target reflec-

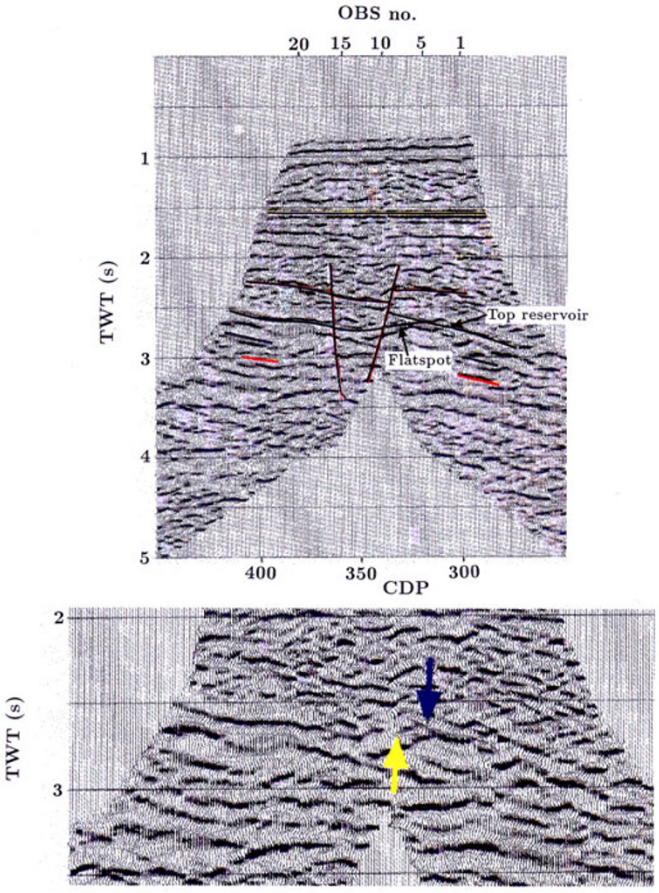

Fig. 17. Interpreted vertical component stack. The arrows on the enlarged part indicate the top of the reservoir and the flatspot, respectively.

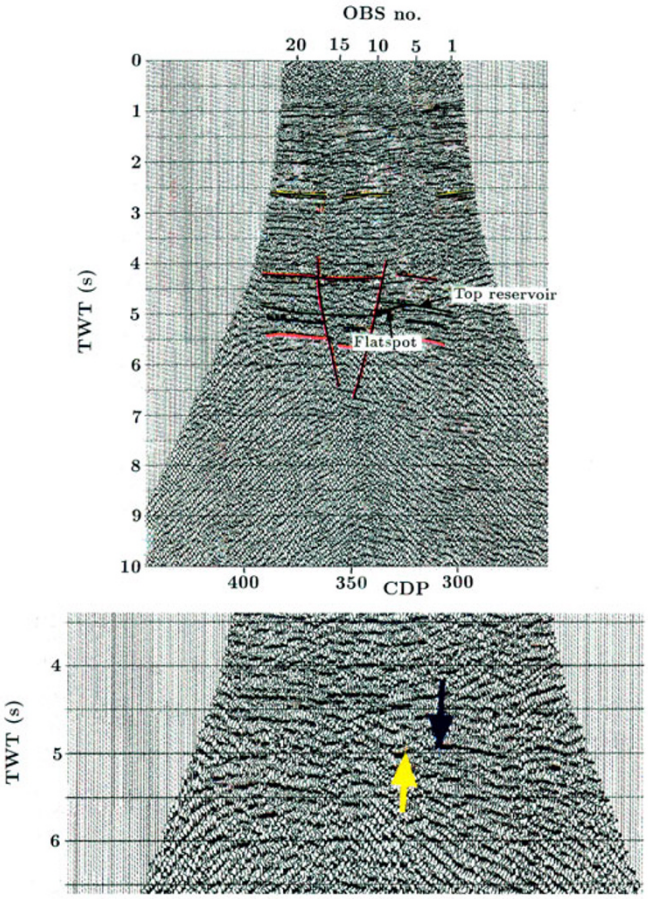

Fig. 18. Interpreted inline horizontal component stack (CCP, same as Fig. 16(b)). The arrows on the enlarged part indicate the top of the reservoir and the flatspot, respectively.

tions for P-to-P data can be seen at 2.6 s and 2.7 s zero-offset traveltimes. These reflections could also be identified on the corresponding OBS V_z-component.

P-to-S converted waves were modeled by varying the V_p/V_s-ratio, and the modeled spikeograms were correlated with the processed OBS inline component. After several iterations, a V_p/V_s-ratio of approximately 2.6 ± 0.1 from the sea-floor to the top of the reservoir provided reasonable traveltime fits between reflections on the modeled OBS data and interpreted reflections on the measured OBS data. The S-velocity for the first two hundred meters below the sea floor was assumed to be just below 200 m/s. The modelling thus indicated which measured reflections correspond to the target area. In the spikeogram in Fig. 19(b), P-to-S converted reflections from the target can be seen at zero-offset traveltimes at approximately 4.75 s and 4.9 s. The modeled zero-offset traveltimes are in reasonable agreement with the traveltimes observed on the processed inline section.

4. Lithology and Fluid Prediction

From the interpreted Z and X component sections (Figs. 17 and 18) it is possible to measure the travel times within layers for both P- and S-waves, and hence calculate the V_p/V_s-ratios for different intervals. If t_S and t_P are the two way travel times measured between two horizons on the X- and Z-sections, respectively, and one assumes that shear waves are generated upon reflection, then;

$$\frac{V_P}{V_S} = \frac{t_S - (t_P/2)}{(t_P/2)}. \tag{3}$$

The travel times were measured on the two sections by means of the "Screen Display" option in ProMAX and the horizons were picked (identically to the interpretation) with the picking tool. As the picks can be snapped to a peak, trough or zero crossing, all three were tried. As well as calculating a direct V_p/V_s-ratio over the flatspot (within the assumed reservoir), the variation in the V_p/V_s-ratio was estimated along the layer in which it is located. The results of the modelling and interpretation show a V_p/V_s-ratio of approximately 2.6 in the overburden, which indicates partly unconsolidated shale, while the V_p/V_s-ratio in the assumed reservoir is approximately 1.8, which indicates more sand dominated facies. Outside the flatspot area within the same stratigraphic layers the V_p/V_s-ratio is estimated to be approximately 2.0. This indicates that hydrocarbons could be present in the assumed reservoir. The lower V_p/V_s-ratio beneath the Intra Campanian unconformity, is also inferred from the modelling of the semi-regional OBS-data (Digranes *et al.*, 2000). It must be emphasized that the uncertainty in the V_p/V_s estimates, that mainly is related to uncertainties in interpretation, is of about the same order as the differences between the obtained values (± 0.1). The interpreta-

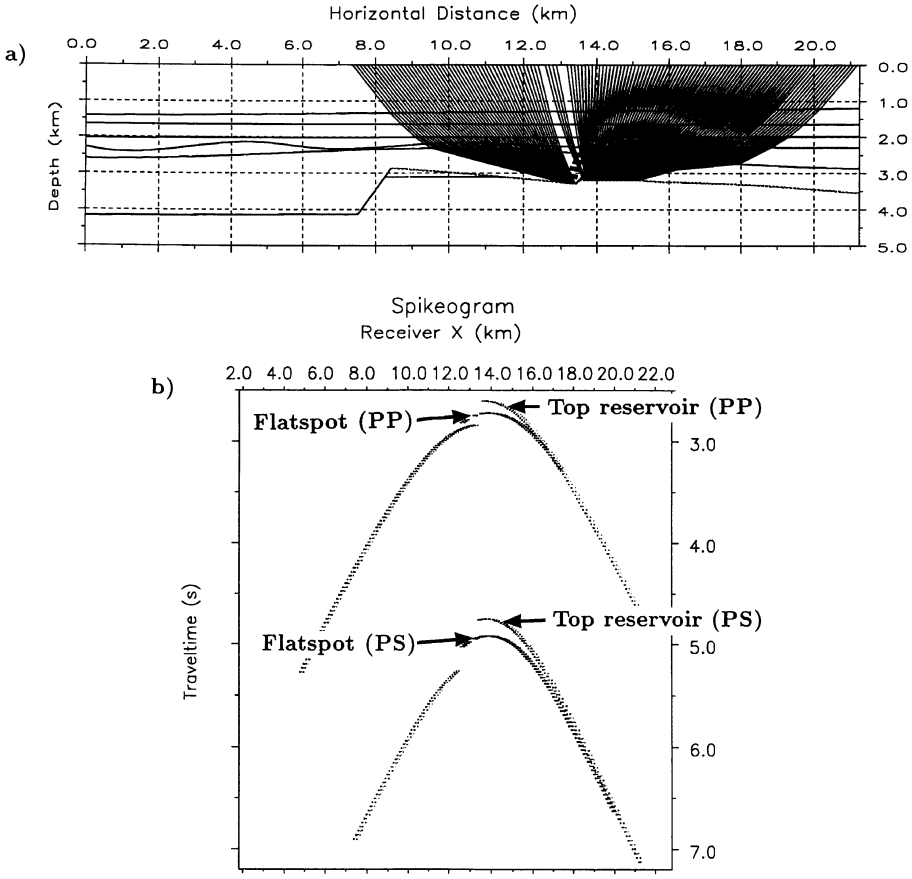

Fig. 19. a) Model (interfaces) with ray-paths reflected from the target area. b) Traveltime curves (spikeogram) of P-P- and P-S-reflections from the top of the reservoir and the flatspot.

tion concerning dating of interfaces, lithology and fluids has been confirmed, however, by recent drilling (the Norwegian Petroleum Directorat, unpublished information).

5. Conclusions

The locally acquired OBS-data from the Vøring basin have been successfully processed by use of conventional reflection data processing methods, and stacked sections have been obtained both for P- and S-waves. The processing was difficult due to the irregular spatial sampling, limiting the pre-stack processing to trace-by-trace tools. A strong offset mute had to be applied to the vertical component due to the presence of strong multiples. These multiples were not present in the horizontal component data, and the application of the mute was hence not necessary for this component. The rotation of the horizontal components proved to be difficult, partly due to lower data quality for these components, and the quality of the stack (S-waves) was not as good as for the data from the vertical component (P-waves). Most of the processing effort was related to the geometry, velocity analysis and rotation of the horizontal components.

The frequency content (resolution) appears to be higher on the horizontal stack than on the corresponding stack from the vertical components. This difference can be contributed to the low S-wave velocity in the interval from the sea-floor to the reservoir-level.

The data have been modeled by ray-tracing, and the V_p/V_s-ratio was estimated to 2.6 from the sea-floor to the top of the assumed reservoir, indicating domination of partly unconsolidated shale. The V_p/V_s-ratio within the reservoir was estimated to 1.8, and within the same stratigraphic layers outside the area of the flatspot the V_p/V_s-ratio was estimated to 2.0. The lower ratio within the reservoir suggests that hydrocarbons could be present.

The calculation of V_p/V_s-ratios presented in this study are based on travel times from the P- and S-wave sections, which are far more robust and reliable than from conventional amplitude analysis. The results have been achieved by use of (only) one simple academic vessel and ocean bottom recorders primarily designed for the studies of earthquakes and regional seismic experiments. We believe that the study demonstrates the large potential more sophisticated experiments (geophone cables, clamped geophones etc.) have in S-wave detection and reduction of risks in hydrocarbon exploration.

It is postulated that these methods will have significant economical impact for Norway, which is the third largest oil and gas producer in the world. Norway's main production is at present focused in the North Sea between Norway and UK, whereas the largest future potential is concidered to be located at the mid-Norway margin (between Møre and Lofoten, Fig. 1). Some prospects have been discovered on the Trøndelag Platform, whereas the Vøring Basin, the target area for this paper, at present is subject to its first round of

exploration.

Furthermore, the acquisition and processing scheme developed may also become important in scientific and commercial lithology and fluid predictions in settings like convergent margins.

Acknowledgments. We are indebted to Prof. M. A. Sellevoll at the Institute of Solid Earth Physics (IFJ), University of Bergen for his support during the planning of the experiment. The crew on R/V Håkon Mosby is greatly acknowledged for their skills and help in all possible situations. We thank further the participating technicians and students from IFJ and the Hokkaido University. We also thank the Norwegian Petroleum Directorate for giving the permission for the experiment and to present part of the reflection profile VB-08-89, S. Vaage and Seres for modelling the air-gun configurations, Geoteam for processing the navigation data, Geco for providing air-chambers for the experiment, and Y. Li from the Hokkaido University for a/d converting parts of the OBS-data. Finally, Statoil is thanked for the permission to present these results, and for economical support.

Appendix A. Geometry Application

In ProMAX several methods can be used for creating the geometry necessary for processing and stacking the data, the simplest being a conventional marine 2D geometry created with the "Marine Geometry" tool. However, for this dataset there were several problems; the receivers were located at irregular intervals on the sea bed, they were stationary for the duration of the shooting, and the shots were not at regular intervals. The geometry was therefore more similar to a land 2D survey, but in order to create this type of geometry with the "Geometry Spreadsheet" or "GMG Geoscribe (2D)" tools, shot coordinates would be needed. These problems were solved by manually generating the geometry by manipulation of trace headers, and then transfering this information from the headers back into ProMAX via the "Extract Database Files" tool. In order to further simplify the process, the source and receiver positions were reversed; the OBS stations were considered as shot points and the shot points as receiver locations. The geometry then appeared more regular to the database, and it is generally easier to work with common OBS gathers when they appear as shots or field files. The header words were created by re-sequencing headers and simple geometric calculations based on the trace co-ordinates. Each common OBS gather was re-numbered with a new field file and the offset related headers were created by binning the offset header already present. The coordinates and surface locations were based on their distance from OBS location 1 and were assumed to be in a single vertical plane (2D). By calculating the distance to the OBS from OBS location 1 and adding 15000 m the source x coordinate was created:

$$sou\_x = \sqrt{(obx\_x - 415409)^2 - (obs\_y - 7435151)^2} + 15000.$$

The traces in each OBS gather were given a receiver x coordinate and a CMP x coordinate by:

$$rec\_x = sou\_s - offset$$
$$cmp\_x = \frac{sou\_x - rec\_x}{2}.$$

Note that the associated y coordinates were set to 0.0. The surface shot point locations were calculated in a similar way, by reference to SP3627 at OBS location 1:

$$sou\_sloc = 3627 + INT\left(\frac{15000 - sou\_x}{25.0}\right)$$
$$rec\_sloc = 3627 + INT\left(\frac{15000 - rec\_x}{25.0}\right)$$
$$cdp\_sloc = 3627 + INT\left(\frac{15000 - cdp\_x}{25.0}\right).$$

In the normal mid-point sense, cmp x can be considered as a point along a CMP line for each trace and can therefore be binned into intervals. Various intervals (from 25 m to 200 m) were tested, and a bin width of 50 m proved to be adequate. The average fold for this bin width, if all offsets are included in the stack, is around 80 and the number of CMP bins is 338, as can be seen in Fig. 7. Discarding traces not contributing to the stack at the target level leaves a fold of stack of around 25. For asymmetric or common conversion point binning of the horizontal components, the calculation of CCP x includes constants derived from the V_p/V_s-ratio. The CCP formula used is:

$$\text{CCP} = \frac{2}{V+1}Source + \frac{2V}{V+1}Receiver$$

where

$$V = \frac{V_P}{V_S}.$$

When the V_p/V_s-ratio equals one, this equation gives normal CMP numbering. A geometry was created for the horizontal component data with a V_p/V_s-ratio of 1.0, 1.75, 2.0, 2.5 and 2.75. As the processing software expects data to have a common mid or depth point number stored as the header word CDP, each dataset that has a geometry applied to it must copy either the CCP or the CMP information into the CDP family of headers. This step was best performed when the "master" dataset was read (the headers only) and the "Extract Geom Files" tool was used. The master dataset was then copied into the work area, and the new geometry was loaded into the trace headers.

Appendix B. Rotation of the Horizontal Components

As there was no compass within the instruments, the orientation of the two horizontal components was unknown, and attempts were thus made to rotate the components into inline (X) and crossline (Y) components. This was performed on the raw-data, and after application of a 250 ms operator and 50 ms gap predictive deconvolution (the same as for the vertical component), as the data were contaminated by low frequency ringing. Figure 6 shows one of the horizontal components of OBS 10 s without any processing. Application of the deconvolution and band pass filtering provide a marked improvement and allows many higher frequency events to be distinguished (Fig. 14).

In order to orient the horizontal components, two different procedures were followed. Firstly, the RMS and average amplitude levels were calculated, and the component containing the highest level of energy was assumed to be closest to the inline direction. Secondly, the polarity of the first arrivals was studied in order to find the azimuths of the components.

Two sets of software were used for this purpose (Sensor Geophysical and ProMAX VSP), both depending strongly on a defined time window having a clean wavelet (a first arrival) to operate on. The Sensor Geophysical software was the simplest to use and outputs a display showing a time lag (for anisotropy) and rotation angle (either positive or negative). However, when the angle (including the polarity) was used to rotate the data the components did not show the expected energy transfer and the results were thus unsuccessful. This could be due to the fact that this software is primarily designed to detect anisotropy characteristics of the data.

The ProMAX VSP software was more difficult to apply as it is designed for data recorded in boreholes, but with some manipulation of the geometry it was possible to use the "3-Component Reorientation" tool. The output is given as a rotation angle for each trace, and it is then possible to average these visually (by transfering them to the ProMAX database) or to use the trace manipulation processes to average them as header values.

As the rotation of the data was not conclusive and did not appear satisfactory for all of the OBSs, both methods were used. Firstly, it was assumed that the component with the maximum energy (i.e. largest RMS level) is the *X* component (Fig. 14) and the component with the minimum energy is the *Y* component (Fig. 15), and secondly, the components were rotated with the angles found. These two *X* component datasets were then processed further with conventional processing tools. It is important to underline that the true inline direction was not needed, as most of the analyzes was based on traveltime information.

References

Caldwell, J., Marine multicomponent seismology, *The Leading Edge*, Nov., 1274–1282, 1999.

Christensen, N. I., Pore pressure and oceanic crustal seismic structure, *Geophys. J. R. Astron. Soc.*, **79**, 411–423, 1984.

Christensen, N. I. and D. M. Fountain, Constitution of the lower continental crust based on experimental studies of seismic velocities in granulite, *Geol. Soc. Am. Bull.*, **86**, 227–236, 1975.

Crampin, S., The scattering of S waves in the crust, *Pure and Applied Geophysics*, **132**, 67–91, 1990.

Digranes, P., R. Mjelde, S. Kodaira, H. Shimamura, T. Kanazawa, H. Shiobara, and E. W. Berg, Modelling shear waves in OBS data from the Vøring basin (Northern Norway) by 2-D ray-tracing, *Pure and Applied Geophysics*, **4**, 611–629, 1996.

Digranes, P., R. Mjelde, S. Kodaira, H. Shimamura, T. Kanazawa, H. Shiobara, and E. W. Berg, Comparison between a regional and semi-regional S-wave model from OBS data in the Vøring basin, N. Norway, *Pure and Applied Geophysics*, 2000 (submitted).

Kanazawa, T., Technical description of TK92-type ocean bottom seismometer, in *Investigation of the Central and Northern Part of the Vøring Basin by Use of Ocean Bottom Seismographs, R/V Håkon Mosby 22 Aug.–24 Sept. 1992, Cruise Report*, edited by R. Mjelde *et al.*, 87 pp., Statoil report, 1993.

Kern, H., Elastic wave velocity in crustal and mantle rocks at high pressure and temperature: The role of high-low quartz transition and of dehydration reactions, *Phys. Earth Planet. Inter.*, **29**, 12–23, 1982.

Mjelde, R., E. W. Berg, A. Strøm, O. Riise, H. Shimamura, T. Kanazawa, H. Shiobara, S. Kodaira, and J. P. Fjellanger, An extensive Ocean Bottom Seismograph survey in the Vøring basin, N. Norway, *First Break*, **14**, 247–256, 1996.

Mjelde, R., S. Kodaira, H. Shimamura, T. Kanazawa, H. Shiobara, E. W. Berg, and O. Riise, Crustal structure of the central part of the Vøring basin, N. Norway, from three-component ocean bottom seismographs, *Tectonophys.*, **277**, 235–257, 1997a.

Mjelde, R., S. Kodaira, P. Digranes, H. Shimamura, T. Kanazawa, H. Shiobara, and E. W. Berg, Comparison between a regional and semi-regional crustal OBS-model in the Vøring basin, N. Norway, *Pure and Applied Geophysics*, **149**, 641–665, 1997b.

Neidell, N. S., Land applications of S waves, *Geophysics: The Leading Edge of Exploration*, 32–44, 1985.

Nur, A. and G. Simmons, The effect of saturation on velocity in low porosity rocks, *Earth Planet. Sci. Lett.*, **7**, 183–193, 1969.

Rodriguez-Suarez, C., R. R. Stewart, and G. F. Margrave, Where does S-wave energy on OBC recordings come from?, 70th Ann. Intl. SEG Meeting, Extended abstract, 2000.

Shimamura, H., OBS technical description, in *Seismiske Undersøkelser av Lofoten Marginen og Refleksjonsseismiske Test-målinger på Mohns Rygg, M/S Håkon Mosby, 29 Juli–19 August, 1988, Cruise Report*, edited by M. A. Sellevoll, 72 pp., Inst. of Solid Earth Physics Report, Univ. of Bergen, 1988.

Shiobara, H., A. Nakanishi, R. Mjelde, T. Kanazawa, E. W. Berg, and H. Shimamura, Precise determination of OBS positions by using acoustic transponders and CTD, *Marine Geophysical Researches*, **19**, 199–209, 1997.

Spencer, J. W. and A. Nur, The effect of pressure, temperature and pore water on velocities in Westerly granite, *J. Geophys. Res.*, **81**, 899–904, 1976.

E. Berg (e-mail: eberg@sbgeo.no), L. Amundsen, A. Morton, R. Mjelde, H. Shimamura, H. Shiobara, T. Kanazawa, S. Kodaira, and J. P. Fjellanger